TITLE PAGE

A high-resolution regional emission inventory of atmospheric mercury and its comparison with multi-scale inventories: a case study of Jiangsu, China

Hui Zhong[1], Yu Zhao[1, 2*], Marilena Muntean[3], Lei Zhang[4], Jie Zhang[2, 5]

1. State Key Laboratory of Pollution Control & Resource Reuse and School of the Environment, Nanjing University, 163 Xianlin Ave., Nanjing, Jiangsu 210023, China

2. Jiangsu Collaborative Innovation Center of Atmospheric Environment and Equipment Technology (CICAEET), Nanjing University of Information Science & Technology, Jiangsu 210044, China

3. European Commission, Joint Research Centre, Institute for Environment and Sustainability, Air and Climate Unit, Via E. Fermi, Ispra, Italy

4. University of Washington-Bothell, 18115 Campus Way NE, Bothell, WA 98011, U.S.A.

5. Jiangsu Provincial Academy of Environmental Science, 176 North Jiangdong Rd., Nanjing, Jiangsu 210036, China

* Corresponding author: Phone: 86-25-89680650; email: yuzhao@nju.edu.cn

ABSTRACT

A better understanding of the discrepancies in multi-scale inventories could give an insight on their approaches and limitations, and provide indications for further improvements; international, national and plant-by-plant data are primarily obtained to compile those inventories. In this study we develop a high-resolution inventory of Hg emissions at $0.05^{o}\times0.05^{o}$ for Jiangsu China using a bottom-up approach and then compare the results with available global/national inventories. With detailed information on individual sources and the updated emission factors from field measurements applied, the annual Hg emissions of anthropogenic origin in Jiangsu 2010 are estimated at 39 105 kg, of which 51%, 47% and 2% were Hg^{0}, Hg^{2+}, and Hg^{P}, respectively. This provincial inventory is thoroughly compared to three downscaled national inventories (NJU, THU and BNU) and two global ones (AMAP/UNEP and EDGARv4.tox2). Attributed to varied methods and data sources, clear information gaps exist in multi-scale inventories, leading to differences in the emission levels, speciation and spatial distributions of atmospheric Hg. The total emissions in the provincial inventory are 28%, 7%, 19%, 22%, and 70% larger than NJU, THU, BNU, AMAP/UNEP, and EDGARv4.tox2, respectively. For major sectors including power generation, cement, iron & steel and other coal combustion, the Hg contents (*HgC*) in coals/raw materials, abatement rates of air pollution control devices (APCD) and activity levels are identified as the crucial parameters responsible for the differences in estimated emissions between inventories. Regarding speciated emissions, larger fraction of Hg^{2+} is found in the provincial inventory than national and global inventories, resulting mainly from the results by the most recent domestic studies in which enhanced Hg^{2+} were measured for cement and iron & steel plants. Inconsistent information on big power and industrial plants is the main source of differences in spatial distribution of emissions between the provincial and other inventories, particularly in southern and northwestern Jiangsu where intensive coal combustion and industry are located. Quantified with Monte-Carlo simulation, uncertainties of provincial inventory are smaller than those of NJU national inventory, resulting mainly from the more accurate activity data of individual plants and the reduced uncertainties of *HgC* in coals/raw materials.

1 INTRODUCTION

Mercury (Hg), known as a global pollutant, has received increasing attention for its toxicity and long-range transport. Identified as the most significant release into the environment (Pirrone and Mason, 2009; AMAP and UNEP, 2013), atmospheric Hg is analytically defined as: gaseous elemental Hg (GEM, Hg^0) that has longest lifetime and transport distance, and reactive gaseous mercury (RGM, Hg^{2+}) and particle-bound mercury (PBM, Hg^p) that are more affected by local sources. Improved estimates in emissions of speciated atmospheric Hg are believed to be essential for better understanding the global transport, chemical behaviors and mass balance of Hg.

Due mainly to the fast growth in economy and intensive use of fossil fuels, China has been indicated as the highest ranking nation in anthropogenic Hg emissions (Fu et al., 2012; Pacyna et al., 2010; Pirrone et al., 2010). Emissions of speciated atmospheric Hg of anthropogenic origin in China have been estimated at both global and national scales. For example, AMAP/UNEP (2013) and Muntean et al. (2014) developed global Hg inventories, which reported national emissions for China for 2010 and from 1970 to 2008, respectively. At national scale, Hg emissions have been estimated based on more detailed provincial information on energy consumption and industrial production. Zhang et al. (2015), Zhao et al. (2015a) and Tian et al. (2015) evaluated the inter-annual trends in emissions for 2000-2010, 2005-2012, and 1949-2012, respectively, to explore the benefits of air pollution control polices, particularly for recent years.

There are considerable information gaps between inventories, attributed mainly to the data of different sources and levels of details. For coal-fired power plants (CPP), as an example, the global inventories by AMAP/UNEP (2013) and Muntean et al. (2014) obtained the national coal consumption from the International Energy Agency (IEA), and they acquired the information of control technologies from the “national comments” by selected experts and World Electric Power Plants database (WEPP), respectively. In the national inventories by Zhang et al. (2015) and Tian et al. (2015), coal consumption of CPP by province was derived from official energy statistics, and the penetrations of flue gas desulfurization (FGD) systems were assumed at provincial level. Zhao et al. (2015a) further analyzed the activity data and emission control levels plant by plant using a “unit-based” database of power sector. Although data of varied sources and levels of details result in discrepancies between inventories, those

discrepancies and the underlying reasons have not been thoroughly analyzed in previous studies, leading to big uncertainty in Hg emission estimation.

Existing global and national inventories could hardly provide satisfying estimates in speciated Hg emissions or well capture the spatial distribution of emissions at regional/local scales, attributed mainly to relatively weak investigation on individual sources. When they are used in chemistry transport model (CTM), downscaled inventories at global/national scales would possibly bias the simulation at smaller scales. Improvement in emission estimation at local scale, particularly for the large point sources is thus crucial for better understanding the atmospheric processes of Hg (Lin et al., 2010; Wang et al., 2014; Zhu et al., 2015). While local information based on sufficient surveys is proven to have advantages in improving the emission estimates for given pollutants like NO_X and PM_{10} (Zhao et al., 2015b; Timmermans et al., 2013), there are currently very few studies on Hg emissions at regional/local scales in China, and the differences of multi-scale inventories remain unclear.

In this work, therefore, we select Jiangsu, one of the most developed provinces with serious air pollution in China, as study area. Firstly, we develop a high-resolution Hg emission inventory of anthropogenic origin for 2010, based on comprehensive review of field measurements and detailed information on emission sources. That provincial inventory is then compared to selected global and national inventories with a thorough analysis on data and methods. Discrepancies in emission levels, speciation, and spatial distributions are evaluated and the underlying sources of the discrepancies are figured out. Finally, the uncertainty of the provincial emission inventory is quantified and the key parameters contributing to the uncertainty are identified. The results provide an insight on the effects of varied approaches and data on development of Hg emission inventory, and indicate the limitations of current studies and the orientations for further improvement on emission estimation at regional/local scales.

2 DATA AND METHODS

2.1 Data sources of multi-scale inventories

As shown in Figure S1 in the supplement, Jiangsu province (30°45′ N-35°20′ N, 116°18′ E-121°57′ E) is located in Yangtze River Delta in eastern China and covers 13 cities. The Hg emissions of Jiangsu are obtained from two approaches: downscaled from global/national inventories, and estimated using a bottom-up method with

information of local sources incorporated.

In global/national inventories, Hg emissions were first calculated by sector based on activity data and emission factors that were obtained or assumed at global, national or provincial level, and were then downscaled to regional domain with finer spatial resolution. Various methods and data were adopted in multi-scale inventories to estimate Hg emissions for different sectors, as summarized briefly in Table S1 in the supplement. Three national inventories were developed by Nanjing University (NJU, Zhao et al., 2015a), Beijing Normal University (BNU, Tian et al., 2015), and Tsinghua University (THU, Zhang et al., 2015), with major activity data at provincial level obtained from Chinese national official statistics. Compared to NJU and BNU inventories that applied deterministic parameters relevant to emission factors, THU developed a model with probabilistic technology-based emission factors to calculate the emissions. Based on international activity statistics at national level, two global inventories for 2010 were developed by the joint expert group of Arctic Monitoring and Assessment Programme and United Nations Environment Programme (AMAP/UNEP, 2013), and Emission Database for Global Atmospheric Research (EDGARv4.tox2, unpublished). AMAP/UNEP inventory developed a new system for estimating emissions from main sectors based on a mass-balance approach with data on unabated emission factors and emission reduction technology employed in different countries. EDGARv4.tox2 inventory calculated the emissions for all the countries by primarily applying emission factors from EEA (2009) and USEPA (2012), combined with regional technology-specific information of emission abatement measures.

2.2 Development of the provincial inventory

In contrast to the downscaling approach, the emissions are calculated plant by plant based on information of individual sources and then aggregated to provincial level in a bottom-up method. We mention the inventory as bottom-up or provincial inventory hereinafter. Information for individual emission sources are thoroughly obtained from Pollution Source Census (PSC, internal data from Environmental Protection Agency of Jiangsu Province). PSC was conducted by local environmental protection agencies, in which the data for individual sources were collected and compiled through on-site investigation, including manufacturing technology, production level, energy consumption, fuel quality, and emission control device.

Differences in total energy consumption and industrial production levels exist between the PSC data and the energy/economic statistics. For example, the coal consumption by power plants in PSC was 6% larger than the provincial statistics for Jiangsu 2010. Compared to the energy and economic statistics that were commonly used in global/national inventories, we believe the plant-by-plant PSC data could provide more detailed and accurate information on specific emitters, particularly for power and industrial plants.

According to the availability of data, anthropogenic sources are classified into three main categories. Category 1 includes coal-fired power plants (CPP), iron & steel plants (ISP), cement production (CEM) and other industrial coal combustion (OIB). Note that the emissions from coal combustion in cement production are not included in CEM but in OIB, following most other inventories included in this paper for easier comparison. The information on geographic location, activity levels (consumption of energy or raw materials) and penetration of air pollution control devices (APCDs) is compiled plant by plant from PSC, with an exception that the technology employed in CEM are obtained from CCA (2011). Category 2 includes nonferrous metal smelting (NMS), aluminum production (AP), municipal solid waste incineration (MSWI) and intentional use sector (IUS: thermometer, fluorescent lamp, battery and polyvinyl chloride polymer production). Geographic location information for those sources is obtained from PSC, while other activity data come from official statistics at provincial level. Category 3 includes emission sources that are not contained in Pollution Source Census: residential & commercial coal combustion (RCC), oil & gas combustion (O&G), biofuel use/biomass open burning (BIO), rural solid waste incineration (RSWI) and human cremation (HC). They are defined as area sources, and the data sources for them are discussed later in this section.

In general, annual emissions of total and speciated Hg are calculated using Eq. (1) and (2), respectively:

$$E = \sum_{n} AL_n \times EF_n \tag{1}$$

$$E_s = \sum_{n} AL_n \times EF_n \times F_{n,s} \tag{2}$$

where E is the Hg emission; AL is the activity levels (fuel consumption or industrial production); EF is the combined emission factor (emissions per unit of activity level); F is the mass fraction of given Hg speciation; n and s represent emission source type

and Hg speciation (Hg^0, Hg^{2+} or Hg^p).

For CPP/OIB and CEM, Eq. (1) can be revised to Eq. (3) and (4) respectively, with detailed fuel and technology information of individual sources incorporated:

$$E_{CPP/OIB} = \sum_t \sum_i \sum_k AL_i \times HgC_k \times RR_t \times (1 - RE_t) \quad (3)$$

$$E_{CEM} = \sum_t \sum_i (AL_{Limstone} \times HgC_{Limstone} + AL_{Other,i} \times HgC_{Other}) \times (1 - RE_t) \quad (4)$$

where HgC is the Hg content of coal consumed in Jiangsu, calculated based on measured Hg contents of coal mines across the country and an inter-provincial flow model of coal transport (Zhang et al., 2015); $HgC_{Limestone}$ and HgC_{Other} represent Hg contents of limestone and other raw materials (e.g. malmstone and iron powder) in cement production, respectively; RR is the Hg release ratios from combustors; RE is Hg removal efficiency of APCDs; $AL_{Limestone}$ and AL_{Other} represent the consumption of limestone and other raw materials in CEM, respectively; i and k represent individual point source and coal type, respectively; t represent APCD type including wet scrubber (WET), cyclone (CYC), fabric filter (FF), electrostatic precipitator (ESP), FGD and selective catalyst reduction (SCR) systems for CPP, and dry-process precalciner technology with dust recycling (DPT+DR), shaft kiln technology (SKT) and rotary kiln technology (RKT) with ESP or FF for CEM. Note the AL for individual CEM plant is calculated based on the clinker and cement production when the information on limestone or other raw materials is missing in PSC.

For ISP, Eq. (1) could be revised to Eq. (5):

$$E_{ISP} = \sum_i (AL_{steel,i} + AL_{iron,i} \times R) \times EF_{steel} \quad (5)$$

where AL_{steel} and AL_{iron} represent crude steel and pig iron production in ISP, respectively; R is the liquid steel to hot metal ratio provided by BREF (2012), converting the production of pig iron to crude steel equivalent; EF_{steel} is the Hg emission factor applied to steel making, obtained from recent domestic tests by Wang et al. (2016).

Activity data for NMS, AP, MSWI, RCC and O&G are derived from national statistics (NMIA, 2011; NSB, 2011a; 2011b), while Hg consumption in IUS are estimated based on the internal association commercial reports that provide national market and economy information collected at http://www.askci.com/. Activity data for MSWI, RSWI and BIO are taken following Zhao et al. (2015a). Other information

including control efficiencies of APCDs, speciation profiles and emission factors inherited from previous studies is summarized in Table S2-S4.

Regarding the spatial pattern of emissions, the study domain is divided into 4212 grid cells with a resolution at 0.05˚×0.05˚. For Categories 1 and 2, emissions are directly allocated into corresponding grid cells according to the locations of individual sources. As considerable errors of plant locations were unexpectedly found in PSC, the geographic location for point sources with emissions more than 15 kg have been corrected by Google Map. As a result, totally 900 plants are relocated, accounting for 14% of all the point sources. For Category 3, emissions are allocated according to the population density in urban areas (RCC) and that in rural areas (BIO and RSWI).

2.3 Sensitivity and uncertainty analysis of emissions

For better understanding the sources of discrepancies between inventories, a comprehensive sensitivity analysis is conducted to quantify the differences between selected parameters used in multi-scale inventories and the subsequent changes in emission estimation for Category 1 sources. The relatively change (*RC*) of given parameter (*j*) in global/national inventories compared to those in the provincial bottom-up inventory, and the changes in emissions for selected source (*n*) when the value of parameter *j* in the bottom-up inventory is replaced by that in global/national inventories ($E_{diff,n}$), can be calculated using Eqs. (6) and (7), respectively:

$$RC_j = (VO_j - VB_j)/VB_j \quad (6)$$

$$E_{diff,n} = EO_n - EB_n \quad (7)$$

where *VB* is the value of parameters in bottom-up inventory; *VO* is the value of parameters in other national/global inventories; *EB* is Hg emissions for given sector in bottom-up inventory; *EO* is Hg emissions for given sector when the values of parameters in bottom-up inventory are replaced by those in other global/national inventories; *j* and *n* represent given parameter and source type, respectively.

In particular, a new parameter, total abatement rate (*TA*), is defined for the sensitivity analysis, combining the effect of the penetrations of APCDs and their removal efficiencies on emission abatement:

$$TA = \sum_t AR_t \times RE_t \quad (8)$$

where *t* represents APCD type; *AR* and *RE* are the application rate and Hg removal

efficiency, with detailed information provided in Table S5 in the supplement.

The uncertainties of speciated Hg emissions at provincial level are quantified using a Monte-Carlo framework (Zhao et al., 2011). Given the relatively accurate data reported in PSC, the probability distributions of activity levels for individual plants of CPP, OIB, ISP and CEM are defined as normal distributions with the relative standard deviations (RSD) set at 10%, 20%, 20% and 20% respectively. As summarized in Table S6 and Table S7 in the supplement, a database for Hg emission factors/related parameters by sector and speciation are established for China, with the uncertainties analyzed and indicated by probability distribution function (PDF). The PDFs of Hg contents in coal mines by province are obtained from Zhang et al. (2015). For Hg content in limestone ($HgC_{Limestone}$), a lognormal distribution is generated with bootstrap simulation based on 17 field tests by Yang (2014), as shown in Figure S2 in the supplement. For the rest parameters, a comprehensive analysis of uncertainties were conducted, incorporating the data from available field measurements as described in Zhao et al. (2015a). Ten thousand simulations are performed to estimate the uncertainties of emissions, and the parameters that are most significant in determination of the uncertainties are identified by source type according to the rank of their contributions to variance.

3 RESULTS AND DISCUSSIONS

3.1 Emission estimation and comparison by sector

3.1.1 The total Hg emissions from multi-scale inventories

Table 1 provides the Hg emissions by sector and species for Jiangsu 2010 estimated from the bottom-up approach. The provincial total Hg emissions of anthropogenic origin are calculated at 39 105 kg, of which 51% released as Hg^0, 47% as Hg^{2+}, and 2% as Hg^P. In general, Categories 1, 2 and 3 account for 90%, 4% and 6% of the total emissions, respectively. CPP and CEM are the biggest contributors to the total Hg (Hg^T) emissions. For Hg^0, Hg^{2+}, and Hg^P, the sectors with the largest emissions are CPP, CEM, and OIB respectively.

To better understand the discrepancies and their sources between various studies, the emissions from multi-scale inventories are summarized in Table 1 for comparison. Among all the inventories, the total emissions in the provincial inventory are the

largest, i.e., 28%, 7%, 19%, 22%, and 70% higher than NJU, THU, BNU, AMAP/UNEP, and EDGARv4.tox2, respectively. The elevated Hg emissions compared to previous studies could be supported by modeling and observation work to some extent. Based on the chemistry transport modeling using GEOS-Chem (Wang et al., 2014), or correlation slopes with certain tracers (CO, CO_2 and CH_4) from ground observation (Fu et al., 2015), underestimation was suggested for the regional Hg emissions of anthropogenic origin in China.

Direct comparison between inventories is unavailable for every sector, as the definition of source categories is not fully consistent with each other. Therefore, necessary assumption and modification are made on source classification for global inventories. In Table 1, CPP, OIB and RCC for EDGARv4.tox2 actually represent the emissions for all the fossil fuel types, and they are 1316, 5342 lower and 986 kg higher than our estimation from coal combustion, respectively. For AMAP/UNEP, the emissions from regrouped stationary combustion (industrial sources excluded), industry, and intentional use and product waste associated sources (see Table 1 for the detailed definition) are respectively 3382, 2032 higher and 3118 kg lower than our estimation with bottom-up method. Figure 1 shows the ratios of the estimated Hg emissions in national/global inventories to those in the provincial inventory by source. The CPP emissions are relatively close to each other, but larger differences exist in some other sources. The estimates for CEM and ISP in provincial inventory are much higher than NJU, BNU and EDGARv4.tox2 inventories, while those for NMS are extremely smaller. The reasons for those differences are analyzed in details in Sections 3.1.2-3.1.4.

3.1.2 Sensitivity analysis for power plants and industrial boilers

Figure 2 (a) and (b) represents the relative changes in given parameters between the provincial and other inventories, and the subsequent differences in Hg emissions for Category 1 sources, using Eqs. (6) and (7), respectively. For CPP, the differences between provincial and national/global inventories are mainly determined by *AL*, *HgC*, *TA*, and *IEF*, as indicated by the calculation methods summarized in Table S1. (Instead of analyzing *HgC* and *RR* separately, integrated input emission factors (*IEF*) were applied in AMAP/UNEP and EDGARv4.tox2.) For activity level (*AL*), the coal consumption data are collected and compiled plant by plant in the provincial inventory, while they were obtained from Chinese official statistics (NSB, 2011b) in

national inventories. As a result, the coal consumptions in NJU and THU inventories are 17% and 6% smaller than our provincial inventory, resulting in 1968 and 760 kg reduction in Hg emission estimate, respectively.

In national and provincial inventories, as mentioned in Section 2, the Hg contents in the raw coal (HgC_{raw}) consumed by province are estimated using an inter-provincial flow matrix for coal transport based on the results of field measurements on Hg contents for given coal mines (Tian et al., 2010; Tian et al., 2014; Zhang et al., 2012). The HgC_{raw} for Jiangsu in THU and our provincial inventory come from Zhang et al. (2012), who merged the results of two comprehensive measurement studies on HgC_{raw} for coal mines across China after 2000, by themselves and USGS (2004), and the average value is calculated at 0.2 g/t-coal. NJU inventory adopted the HgC_{raw} of 0.169 g/t-coal from Tian et al. (2010), while BNU inventory determined HgC_{raw} at 0.25 g/t-coal with a bootstrap simulation based on a thorough investigation on published data (Tian et al., 2014). HgC_{raw} in NJU and BNU inventories are 15% smaller and 25% higher than that in provincial inventory, leading to differences of 1746 and 2816 kg in Hg emissions, respectively. Given the large differences in HgC_{raw} between countries, global inventories applied national specific IEF based on the domestic tests (UNEP, 2011b; Wang et al., 2010). The IEFs for China applied in AMAP/UNEP and EDGARv4.tox2, without considering the regional differences in HgC_{raw}, are 26% and 28% lower than that in provincial inventory (recalculated with HgC_{raw} and *RR*). As regional HgC_{raw} differs a lot from the national average and could be largely influenced by the data selected, big discrepancy might exist when national value is applied in regional inventory, and more regional-specific measurements are suggested for reducing the uncertainty.

Total abatement rate (*TA*) of APCDs installed for CPP is calculated at 57% in the provincial inventory, 6.7 % and 8.2% smaller than that in THU and AMAP/UNEP inventories, respectively, and 12% larger than that in NJU inventory. The differences result mainly from the varied removal efficiencies (*RE*) and application ratios (*AR*), as shown in Table S5. For *RE*, local tests on FF, ESP+FGD and SCR+ESP+FGD were conducted by JSEMC (2013) and Xie and Yi (2014), and the results (provided in Table S2) are applied in the provincial inventory. From investigation on individual plants, the *AR* of FGD systems with relatively large benefits on Hg removal was underestimated in NJU and overestimated in THU inventory. In the AMAP/UNEP inventory, relevant parameters were obtained from national comment, and elevated *TA*

was estimated due to the larger *AR* of FF and FGD and the higher *RE* of FGD+ESP compared to those obtained from detailed source investigation in the provincial inventory.

For OIB, the comparison of *HgC* is similar to that for CPP. *AL* from PSC in provincial inventory is very close to that in THU inventory obtained from NSB (2011b), while *AL* in NJU inventory was much lower as the coal consumption of CEM and ISP were excluded. The *RR* from industrial boilers in this work is estimated at 82% based on domestic measurements (Wang et al., 2000; Tang et al., 2004), much lower than the result in THU inventory measured by Zhang et al. (2012), i.e., 95% for stoker fired boiler. Given the limited samples in both inventories, large uncertainty exists in *RR* of industrial boilers. Compared to the provincial inventory, *ARs* of ESP and FGD were clearly underestimated in NJU and THU inventories (Table S5), hence the *TA* in NJU was calculated 23% smaller than that in provincial inventory, leading to a 747 kg increase in Hg emission estimate. In THU inventory, however, the much higher RE of WET reduced the difference between national and provincial inventories, and *TA* in THU inventory was only 2% smaller than the provincial one.

3.1.3 Sensitivity analysis for cement and iron & steel industries

For CEM, both the provincial and THU inventories adopted the data from Yang (2014), who measured provincial Hg contents in raw materials (limestone and other raw materials) and Hg removal efficiency of DPT+DR in China. For *AL*, the limestone consumption were calculated based on the clinker and cement production of individual plants in the provincial inventory, while THU relied on cement production at provincial level, leading to 13% smaller in *AL* and 1019 kg reduction in Hg emission estimate. In addition, consumption of other raw materials for CEM were ignored in THU inventory, leading to 1223 kg smaller in emission estimate compared to the provincial inventory. According to on-site survey by Yang (2014), fly ash is 100% reused in DPT+DR, thus the technology minimizes the Hg removal by dust collectors (ESP or FF). The *AR* of DPT+DR in THU was estimated at 82% at national average level, while it reaches 89% in Jiangsu based on detailed provincial statistics (CCA, 2011). Hence the *TA* employed in THU is 25% larger than that in provincial inventory, resulting in 259 kg underestimation in Hg emissions. NJU and AMAP/UNEP inventories failed to characterize the poor control of Hg from DPT+DR. *EFs* applied in NJU came from early domestic measurements on rotary and shaft kiln

(Li, 2011; Zhang, 2007), ignoring the recent penetration of DPT+DR. In AMAP/UNEP inventory, an effective Hg capture of 40% was generally assumed for China's cement plants taking only the use of ESP and FF into account. The *TA* was estimated 215% larger than that in the provincial inventory, resulting in 2253 kg reduction in Hg emission estimate. EDGAR applied uniform emission factor (UEF) of 0.065g/t-clinker from EEA (2009), 32% lower than the average *EF* in the provincial inventory. BNU developed S-shaped curves to estimate the time-varying dynamic emission factors for non-coal combustion sector, based on the assumption of a gradually declining trend in *EFs* along with increased controls of APCDs. As mentioned above, however, the trend was not suitable for CEM due to the penetration of DPT+DR. Thus UEF of 0.02 g/t-cement estimated in BNU might result in underestimation in Hg emissions, e.g., 7261 kg smaller than our provincial inventory.

For ISP, difficulty exists in emission estimation due to various Hg input sources and complex production processes, and there is no consistent method in multi-scale inventories so far. It was found that raw material production (limestone and dolomite), coking, sintering and pig iron smelting with blast furnace account for most Hg emissions in typical ISP in China (Wang et al., 2016). In our study, 11 factories containing those processes are collected in PSC, and the emissions factors of 0.043 and 0.068 g/t-crude steel from Wang et al. (2016) are applied to plants with and without raw material production, respectively. In other inventories, very few results from domestic measurements were applied for Hg emission estimation for ISP in China. NJU took only coal combustion into account, and thus underestimated the emissions for the sector by neglecting the Hg input along with iron ore, limestone and other raw materials. THU applied an emission factor of 0.04 g/t from Pacyna et al. (2010) for crude steel production. Besides difference in emission factors, THU did not count the pig iron production in *AL* estimation, thus *AL* in THU inventory is 29% lower than that in the provincial inventory, resulting in 1615 kg reduction in Hg emission estimate. Average *EF* in AMAP/UNEP was estimated at 0.039 g/t-pig iron by combining the input factor (0.05g/t-pig iron) calculated with a mass balance method (UNEP, 2011a; BREF, 2012), and the removal effects of APCDs. For comparison, *EF* used in our provincial inventory was recalculated at 0.064 g/t-pig iron based on the hot metal charging ratio (*R* in Eq. (5); BREF, 2012). Lower *EF* in AMAP/UNEP can partly be attributed to the overestimated *AR* of APCDs in ISP without considering the gradual penetration of dust recycling as in CEM.

In general, the detailed activity and technology information including manufacturing procedures and APCDs were investigated for individual plants in our provincial inventory to improve the emission estimation, in contrast to previous inventories that applied simplified or regional-average data. However, some crucial parameters, e.g., Hg contents in coal and limestone, and Hg removal efficiencies of APCDs, are still unavailable at plant level due to lack of measurements. Such limitation indicates the necessity of more efforts on plant-specific emission factors, and also motivates the uncertainty analysis for the provincial inventory, as presented in Section 3.4.

3.1.4 Comparisons of emissions for Categories 2 and 3

For Categories 2 and 3, differences also exist in *EF* and *AL* between inventories. For example, an emission factor of 0.22 g/t-waste combusted for MSWI based on domestic tests (L. Chen et al., 2013; Hu et al., 2012) is applied in the provincial inventory, while THU applied 0.5 g/t from UNEP (2005), resulting in a difference of 1024 kg in emission estimate. For primary Cu production, the provincial inventory applied the emission factor of 0.4g/t-Cu from Wu et al. (2012), who incorporated the results of available field measurements and the penetrations of different smelting processes in China. BNU, however, applied a much higher emission factor at 8.9 g/t-Cu estimated by using an S-shaped curve based on international results (Habashi, 1978; Nriagu, 1979; Pacyna, 1984; Pacyna and Pacyna, 2001; Streets et al., 2011; EEA, 2013). In NJU inventory, the emissions from NMS and IUS were estimated much higher than the provincial inventory, attributed largely to the different sources of activity data. For NMS, activity levels in NJU and provincial inventories were obtained from NSB (2011c) and NMIA (2011), respectively. While NMIA (2011) provides the information on the production of primary nonferrous metal (the major source of Hg emissions for NMS), the secondary production were included in NSB (2011c), leading to possible overestimate in *AL* and thereby Hg emissions. For IUS, provincial Hg consumption was allocated from the national total use weighted by GDP in NJU inventory, while the data are directly derived for Jiangsu from internal industrial report in the provincial inventory. In the global inventories, moreover, all the emissions for Categories 2 and 3 in Jiangsu were downscaled from national estimations attributed to lack of provincial information, and big bias could be expected. For example, the large discrepancy for intentional use and product waste

associated sources between downscaled global and provincial inventories is likely attributed to the overestimation in emissions from artisanal and small-scale gold mining (ASGM) by global inventory (not included in Table 1 as no ASGM was found by local source investigation).

3.2 Hg speciation analysis of multi-scale inventories

Besides the total emissions, Hg speciation has a significant impact on the distance of Hg transport and chemical behaviors. Table 2 summarizes the mass fractions of Hg species in emissions by sector for multi-scale inventories.

In general, as shown in Table 2, reduced Hg^0 but enhanced Hg^{2+} is estimated as the spatial scale gets smaller. This can be mainly explained by the use of domestic measurement results on Hg speciation for CEM, ISP and MSWI in the provincial inventory. For CEM, the Hg^{2+} mass fraction for the dominating DPT+DR technology tends to reach 75% based on available measurements (Yang, 2014), leading to a much larger fraction of Hg^{2+} emissions in the provincial inventory. In contrast, speciated Hg emissions were calculated using the same speciation profiles as those for coal combustion in NJU inventory or the uniform profile ignoring the effects of APCDs in AMAP/UNEP inventory. For ISP, heterogeneous Hg oxidation can be enhanced by the high concentration of dust and existence of Fe_2O_3 in the flue gas during sintering process, leading to large Hg^{2+} fraction for the sector reaching 66% (Wang et al., 2016). For MSWI, results of domestic measurements (L. Chen et al., 2013; Hu et al., 2012) were applied in the provincial and NJU inventories, elevating the Hg^{2+} fraction compared to THU and AMAP/UNEP inventories that applied a global uniform speciation profile without consideration of regional difference. It should be noted, however, that uncertainty exists in the estimation of speciated emissions at small spatial scale, attributed mainly to the limited samples in domestic measurements on CEM and ISP.

As mentioned above, the “universal” profiles were applied for many sectors in AMAP/UNEP inventory, ignoring the effects of various types of APCDs on Hg speciation, particularly for coal combustion. However, the fate of Hg released to atmosphere can primarily be affected by the removal mechanisms of APCDs. As shown in Table 3, for example, Hg^0 mass fractions for ESP+FGD and FF+FGD tend to be high reaching 83% and 78%, respectively, attributed to the relatively strong removal effects of APCDs on Hg^{2+} and Hg^p. Once SCR is applied, an increase of Hg^{2+}

fraction can be observed, as the catalyst in SCR system can accelerate the conversion of Hg^0 to Hg^{2+} (Wang et al., 2010). In addition, Hg^0 can also be oxidized to Hg^{2+} in FF attributed to specific chemical composition in flue gas (chlorine, for example) and to high temperature (Wang et al., 2008; He et al., 2012). In contrast to global inventories, therefore, national and provincial inventories take the effects of different APCDs into account. Summarized in Table 3, considerable differences exist in the speciation profiles for typical APCDs between national and provincial inventories, attributed mainly to the various data used from domestic field measurements. Excluding the measurement results on WET (Zhang et al., 2012), NJU assumed same species profile for WET and CYC, and thereby largely underestimated the mass fraction of Hg^0 for OIB where WET is widely applied. Besides, the penetrations of APCDs are also crucial in determination of speciated Hg emissions. As indicated in Table 3, with similar speciation profiles for FGD applied between multi-scale inventories, the difference in Hg speciation is relatively small for CPP between inventories, given the relatively accurate and transparent information on FGD penetration in CPP. For OIB, however, the difference in Hg speciation is significantly elevated, as large diversity in APCDs penetration is found between multi-scale inventories, as shown in Table S5. With the penetration of FF and ESP highly underestimated, for example, THU provided a lower estimation in Hg^{2+} fraction compared to other inventories.

3.3 Comparisons of spatial patterns of emissions between multi-scale inventories

Figure 3 presents the spatial distributions of total and speciated Hg emissions in Jiangsu province at 0.05˚×0.05˚. Similar patterns are found between species. Relatively high emissions are distributed over northwestern and southern Jiangsu, resulting from intensive coal combustion, and cement and iron & steel production, as indicated in Figure S1 in the supplement. As an important energy base, Xuzhou in northwestern Jiangsu contains a large number of coal combustion sources, while great energy demand exists in southern Jiangsu attributed to developed economy and intensive industry. For cement production, as an example, the clinker manufacture plants that dominate the Hg emissions compared to the subsequent mixing stage (UNEP, 2011a), are mainly located in southern Jiangsu, depending on the distribution of limestone resources.

In order to compare the spatial distribution of provincial inventory to that of NJU, THU, AMAP/UNEP and EDGARv4.tox2 inventories, we upscale the gridded

provincial emissions from 0.05˚×0.05˚ to the resolutions of 0.125˚×0.125˚, 36×36km, 0.5˚×0.5˚ and 0.1˚×0.1˚ respectively. Differences in gridded Hg^T emissions for Jiangsu between the upscaled provincial inventory and other multi-scale inventories are presented in Figure 4. Although selected sources were identified as point sources in global/national inventories, e.g., CEM in NJU and THU, ISP in EDGARv4.tox2, and CPP in all the inventories, the emission fraction of point sources (Categories 1 and 2) is significantly elevated to 92% in the provincial inventory. In particular, the emissions from point sources of which the geographic information were corrected account for 78% of total emissions in the province.

As illustrated in Figure 4, differences in gridded emissions between provincial and other inventories NJU, THU, AMAP/UNEP and EDGARv4.tox2 are respectively in the ranges of -760~+4135 kg, -1429~+3217 kg, -1424~+3043 kg and -1078~+3895 kg. Grids with differences more than 400 kg/yr are commonly distributed in southern and northwestern Jiangsu, and coincide well with the locations of point sources with relatively large emissions in the provincial inventory. It can be indicated that differences in spatial patterns of Hg emissions come mainly from the inconsistent information of big point sources between the provincial inventory and national/global inventories. For CPP, AMAP/UNEP obtained information of identified facilities from Wikipedia (http://en.wikipedia.org/wiki/List_of_power_stations_in_Asia), and failed to include a number of coal-fired power plants built in recent years (Steenhuisen et al., 2015). For EDGARv4.tox2, proxy data (e.g., electricity production) from Carbon Monitoring Action (CARMA, http://carma.org/blog/carma-notes-future-data/) are used to allocate Hg emissions. Although CARMA incorporates all the major disclosure databases, uncertainties exist in certain individual plants attributed to lack of information on geographical locations and control technologies. Moreover, as the most updated information in CARMA was collected in 2009, EDGAR had to predict the emissions of CPP for 2010, and could not fully track the actual changes in the sector, e.g., operation of new-built units, or shutting down the small ones. Similarly, NJU and THU obtained the information of power units from a relatively old database (Zhao et al., 2008), and made further assumptions on activities and penetrations of APCDs to update the emissions of individual plants. As a result, in general, larger emissions are found in the provincial inventory than other inventories in southern Jiangsu where big power plants are located, particularly in Nanjing and northern Suzhou. As detailed information at plant level is unavailable for each inventory, we

speculate the discrepancy resulted mainly from the underestimation (or missing) in coal consumption in previous electric power generation databases that other inventories relied on, and from the use of regional/national-average information on APCD penetration by certain inventories (e.g., THU and AMAP/UNEP). The comparison in northwestern Jiangsu is less conclusive: the emissions in the areas with big power plants were estimated lower in provincial inventory than AMAP/UNEP (Figure 4(c)). Such difference, however, result not only from the varied estimations in CPP emissions but also from discrepancy in other sources, e.g., intensive emissions from industrial sources in the area in AMAP/UNEP. For ISP and CEM, similarly, higher emissions were estimated by the provincial inventory for areas with big plants in Zhenjiang, Suzhou and Changzhou in southern Jiangsu. In contrast to the provincial inventory that investigated the activities of each manufacturing processes for individual plants, the emissions in national inventories (THU and NJU) were allocated based only on the production of plants, ignoring the effects of manufacturing technologies on emissions. Moreover, some CEM and ISP plants were missed in those national inventories, leading to underestimation in emissions for corresponding regions. When the national inventory was applied in CTM, the simulated concentrations of Hg^T were usually lower than the observation at rural sites in eastern China (Wang et al., 2014). Since many big plants are being moved from urban to rural areas (Zhao et al., 2015b; Zhou et al., 2016), improvement in model performance could be expected when the elevated emissions in rural areas are estimated and used for CTM, incorporating the accurate information of individual big plants.

With much fewer big emitters, discrepancies in gridded emissions for other part of Jiangsu resulted largely from the allocation of emissions as area sources in national and global inventories. For example, in spite of an estimation of 8496 kg smaller than the provincial inventory in total emissions, NJU inventory applied proxies (e.g., population and GDP) to allocate the emissions except those from CPP, resulting in higher emissions in central and most part of northern Jiangsu (Figure 4(a)). Similar patterns are also found for THU (Figure 4(b)) and AMAP/UNEP (Figure 4(c)) compared to provincial inventory.

Besides the total emissions, differences in spatial distribution of speciated Hg emissions between multi-scale inventories are presented in Figure S3 in the supplement. The various patterns for species are largely influenced by the distribution of different types of big point sources, as the speciation profiles vary significantly

between source types in the national and provincial inventories (Table 2). Compared to other inventories, larger Hg^0 emissions were found in the provincial inventory in southern Jiangsu (particularly Zhenjiang and Taizhou) where CPPs with large fraction of Hg^0 are intensively located. Elevated Hg^{2+} emissions were dominated by intensive CEM industry in Changzhou, Wuxi and Zhenjiang in southern Jiangsu, as the Hg^{2+} fraction of CEM reaches 73% in the provincial inventory. Differences in Hg^P emissions between inventories in central Jiangsu are closely related with the locations of OIB plants, attributed mainly to the relatively poor understanding of the particle control and thereby Hg^p release of OIB. The emissions in the provincial inventory is larger than THU but smaller than AMAP/UNEP, as the Hg^p mass fraction of OIB was assumed at 2% in THU while it reached 10% in AMAP/UNEP (Table 2).

The vertical distribution of Hg releases, which is crucial for the transport range of atmospheric Hg, is also analyzed. Four groups of release height are defined: 0-58m, 58-141m, 141-250m and >250m. Based on the detailed information of emission sources, the fractions of Hg releases into the four groups for CPP are 2%, 66%, 31%, and 1%, respectively, and the analogue numbers for OIB, ISP, and CEM are 85%, 13%, 2%, and 0%; 4%, 44%, 12%, and 4%; and 6%, 94%, 0%, and 0%, respectively. The release heights for rest sources are uniformly assumed at the range of 0-58m. As a result, the fractions of total Hg emissions in the four groups are estimated as 35%, 53%, 11% and 1%. In AMAP/UNEP inventory, as a comparison, the fractions at the height of 0-50m, 50-150m and >150m were estimated at 23%, 53% and 24% respectively, with larger share in Hg emitted over 150m than that in our provincial inventory. The smaller fraction of Hg emissions under 150m and larger fraction of Hg^{2+} as discussed in Section 3.2 in the provincial inventory are expected to result in more local deposition and less long-range transport compared to previous inventories when they are applied in CTM. The re-emissions of legacy Hg could then be enhanced and make a significant contribution to atmospheric Hg concentrations, as indicated by Zhu et al. (2012).

3.4 Uncertainty of the provincial inventory

As summarized in Table 4, the uncertainties of speciated Hg emissions in the provincial inventory are estimated at -24%~+82% (95% confidence intervals (CI) around central estimates), -34%~+99%, -23%~68%, and -34%~+270% for Hg^T, Hg^0, Hg^{2+} and Hg^p, respectively. For comparison, the uncertainties of Jiangsu emissions

from major sectors including CPP, CEM, ISP and OIB in NJU inventory are recalculated following Zhao et al. (2015a) and provided in Table 4 as well. The uncertainties for major sources in the provincial inventory were smaller than those in NJU inventory, attributed largely to the bottom-up approach used in provincial inventory with more accurate information on activity levels and APCDs applications for individual plants of Category 1. In addition, with more field measurements on Hg contents in coal and limestone incorporated, the uncertainties of HgC_{raw} and $HgC_{Limstone}$ are significantly reduced, resulting from the mechanism of error compensation when HgC_{raw} of coals produced in different provinces are taken into account in the inter-provincial flow model for coal transport, and from the success in bootstrap simulation, respectively. As a result, the uncertainties of emissions from CPP, OIB and CEM are effectively reduced in the provincial inventory.

The parameters contributing most to uncertainties and their contributions to the variance of corresponding emission estimates are summarized by sector in Table S8 in the supplement. For CPP and OIB, parameters related to emission factors contribute most to the uncertainties of Hg^T emissions, including the HgC_{raw} in provinces with largest contribution to the input of coal consumed in Jiangsu (i.e., Shaanxi and Inner Mongolia), and the removal efficiencies (*RE*) or release ratios (*RR*) of Hg for typical APCD (ESP+FGD) and combustor type (grate boiler). HgC_{raw} of coals produced in Shaanxi and Inner Mongolia that collectively accounted for 34% of coal consumption in Jiangsu, contributed 26% and 18% to the uncertainties of Hg emissions for CPP, and 15% and 11% to those for OIB, respectively. It is thus essential to conduct systematic and synergetic measurements on HgC_{raw} in different regions (particularly those with large coal production) to constrain the uncertainties of Hg emission estimation for coal combustion sources, at both regional and national scales. Given the wide application of ESP+FGD in CPP (70% in coal consumption), $RE_{ESP+FGD}$ is estimated to contribute 20% to Hg emissions from CPP. Local measurements on *RE* of typical APCDs, which have started in Jiangsu (JSEMC, 2013; Xie and Yi, 2014), are expected to potentially improve the Hg emission estimation at regional level. Although applied in 92% of OIB plants in Jiangsu, there are very few studies on Hg release rate of grate boiler, resulting in a contribution of 5% to the emission uncertainty. For CEM, $HgC_{Limestone}$ dominates the uncertainties of Hg emissions, with the contribution estimated at 84%. Attributed to lack of detailed information, provincial average of $HgC_{Limestone}$ with the lognormal distribution fitted through

bootstrap simulation based on available measurements (Figure S2 and Table S6) was uniformly applied for all the individual plants, leading to the enhanced contribution to the uncertainty. For ISP, *EF* of limestone and dolomite production contributes 60% to Hg emissions, as the process is estimated to account for 88% of emissions from the entire sector. In addition, *AL* from the biggest ISP factory, which accounted for 40% and 75% of pig iron and crude steel production for the whole province, respectively, contributes 24% to the total uncertainty of ISP sector. The result indicates a necessity of specific investigation on super emitters. For rest sources, MSWI, BIO and O&G are the biggest sources for Hg^T emissions, and *EFs* of those types of sources thus contribute most to the emission uncertainty.

In most cases, parameters with big contribution to uncertainty of Hg^T also play crucial roles in uncertainty of speciated emissions. Moreover, the speciation profiles for typical source types and APCDs are identified as key parameters to the uncertainties of speciated emissions as well. For example, the mass fraction of Hg^{2+} from ESP+FGD, and that of Hg^p from ESP are the biggest contributors to uncertainties of Hg^{2+} and Hg^p emissions from CPP, respectively. For OIB, the mass fraction of Hg^p from sources without any control is much higher than those with APCDs (Table 3), thus it plays an important role in the emission uncertainty, with the contribution estimated at 35%. For CEM and ISP, studies on speciation profiles are limited so far, and the speciation profiles for DPT+DR and ISP plants contribute largely to uncertainties of speciated emissions.

4 CONCLUSIONS

Taking Jiangsu province in China as an example, the discrepancies and their sources of atmospheric Hg emission estimations in multi-scale inventories applying varied methods and data are thoroughly analyzed. Using a bottom-up approach that integrates best available information of individual plants and most recent field measurements, the total Hg emissions in Jiangsu 2010 are estimated larger than any other national/global inventories. CPP, ISP, CEM and OIB collectively accounted for 90% of the total emissions. Comparisons between available studies demonstrate that the information gaps of multi-scale inventories lead to big differences in Hg emission estimation. Discrepancies in emissions between inventories for the above-mentioned major sources come primarily from various data sources for activity levels, Hg

contents in coals and total abatement effects of APCDs. Notable increase in Hg^{2+} emissions is estimated with the bottom-up approach compared to other global/national inventories, attributed mainly to the adoption of domestic measurement results with elevated mass fraction of Hg^{2+} for CEM, ISP and MSWI. Inconsistent information of big point sources lead to large differences in spatial distribution of emissions between provincial and other inventories, particularly in southern and northwestern of the province where intensive coal combustion and industry are located. Improved estimates in emission level, speciation and spatial distribution are expected to better support the regional chemistry transport modeling of atmospheric Hg. Compared to the national inventory, uncertainties of Hg emissions are reduced in provincial inventory using the bottom-up approach.

The method developed and demonstrated for Jiangsu could potentially be promoted to other provinces, particularly for those with intensive industrial plants. As estimated in this work, for example, cement and iron & steel industries were the two most important sectors of which the Hg emissions were significantly underestimated by previous inventories for Jiangsu. The underestimations came mainly from the ignorance of high Hg release ratio of precalciner technology with dust recycling, and application of relatively low emission factors for steel production. We could thus cautiously infer that Hg emissions might be underestimated for China's other regions with intensive cement and steel industries in previous inventories. For power plants and industrial boilers, however, the Hg emissions were influenced largely by Hg contents in coal and APCDs application. Whether the emissions of those sources were underestimated or not for other parts of the country could hardly be judged unless detailed information gets available for the regions. Extensive and dedicated measurements are urgently suggested on Hg contents in coal/limestone and removal efficiency of dominating APCDs to further improve the emission estimation at regional/local scales, and eventually for the whole country.

DATA ACCESS

The gridded Hg emissions for Jiangsu province 2010 at a horizontal resolution of $0.05^{o} \times 0.05^{o}$ can be downloaded at http://www.airqualitynju.com/En/Data/List/Data%20download.

ACKNOWLEDGEMENT

This work was sponsored by the Natural Science Foundation of China (41575142), Natural Science Foundation of Jiangsu (BK20140020), Jiangsu Science and Technology Support Program (SBE2014070918), and Special Research Program of Environmental Protection for Commonweal (201509004). We would like to acknowledge Hezhong Tian from Beijing Normal University and Simon Wilson from UNEP/AMAP Expert Group for the detailed information on national/global Hg emission inventories.

REFERENCES

AMAP/UNEP: Technical Background Report to the Global Atmospheric Mercury Assessment, Arctic Monitoring and Assessment Programme, Oslo, Norway/UNEP Chemicals Branch, Geneva, Switzerland, 159 pp., 2008.

AMAP/UNEP: Technical Background Report for the Global Mercury Assessment, Arctic Monitoring and Assessment Programme, Oslo, Norway/UNEP Chemicals Branch, Geneva, Switzerland, 263 pp., 2013.

Best Available Techniques Reference Document (BREF) for Iron and Steel Production, Industrial Emissions Directive 2010/75/EU. (Integrated Pollution Prevention and Control), European Commission, March, 2012, online at: http://eippcb.jrc.ec.europa.eu/reference/BREF/IS_Adopted_03_2012.pdf.

Chen, C., Wang, H. H., Zhang, W., Hu, D., Chen, L., Wang, X. J.: High-resolution inventory of mercury emissions from biomass burning in China for 2000-2010 and a projection for 2020, J. Geophys. Res., 118, 12248-12256, 2013.

Chen, L., Liu, M., Fan, R., Ma, S., Xu, Z., Ren, M., He, Q.: Mercury speciation and emission from municipal solid waste incinerators in the Pearl River Delta, South China, Sci. Total Environ., 447, 396–402, 2013.

China Cement Association (CCA) : China cement almanac, China Building Industry Press, 2011.

Fu, X. W., Feng, X. B., Sommar, J., Wang, S. F.: A review of studies on atmospheric mercury in China, Sci. Total Environ, 421–422, 73–81, 2012.

Fu, X. W., Zhang, H., Lin, C. J., Feng, X. B., Zhou, L. X., Fang, S. X.: Correlation slopes of GEM / CO, GEM / CO2, and GEM / CH4 and estimated mercury emissions

720 in China, South Asia, the Indochinese Peninsula, and Central Asia derived from
721 observations in northwestern and southwestern China, Atmos. Chem. Phys., 15,
722 1013–1028, 2015.
723 European Environment Agency (EEA): EMEP/EEA air pollutant emission inventory
724 guidebook 2009, Technical report No 9/2009, available online at:
725 http://www.eea.europa.eu/publications/emep-eea-emission-inventory-guidebook-2009
726 European Environment Agency (EEA): EMEP/EEA air pollutant emission inventory
727 guidebook 2013, available online at:
728 http://www.eea.europa.eu/publications/emep-eea-guidebook-2013
729 Habashi, F.: Metallurgical plants: how mercury pollution is abated, Environ. Sci.
730 Technol., 12, 1372-1376, 1978.
731 He, Z. Q., Kan, Z. N., Qi, L. M., Han, X. F.: Analysis to mercury removal
732 performance test of bag-type dust collector, Inner Mongolia Electric Power, 30 (1),
733 0040-0042, 2012 (in Chinese).
734 Hu, D., Zhang, W., Chen, L., Ou, L. B., Tong, Y. D., Wei, W., Long, W. J., Wang, X.
735 J.: Mercury emissions from waste combustion in China from 2004 to 2010, Atmos.
736 Environ., 62, 359–366, 2012.
737 Jiangsu Environment Monitoring Center (JSEMC): Research on mercury emissions in
738 flue gas of coal-fired power plants in Jiangsu Province, Interim report, 2013 (in
739 Chinese).
740 Li, W.: Characterization of Atmospheric Mercury Emissions from Coal-fired Power
741 Plant and Cement Plant (Master Thesis), Xi'nan University, Chongqing, China, 2011
742 (in Chinese).
743 Lin, C. J., Pan, L., Streets, D. G., Shetty, SK., Jang, C., Feng, X., Chu, H. W., Ho, T.
744 C.: Estimating mercury emission outflow from East Asia using CMAQ-Hg, Atmos.
745 Chem. Phys., 10(4), 1853-1864, 2010.
746 Muntean, M., Janssens-Maenhout, G., Song, S., Selin, N. E., Olivier, J. G. J.,
747 Guizzardi, D., Maas, R., Dentener, F.: Trend analysis from 1970 to 2008 and model
748 evaluation of EDGARv4 global gridded anthropogenic mercury emissions,
749 Sci. Total Environ., 494–495, 337–350, 2014.
750 Nriagu, J. O.: Global inventory of natural and anthropogenic emissions of trace metals
751 to the atmosphere, Nature, 279, 409-411, 1979.
752 National Statistical Bureau of China (NSB): China Statistical Yearbook, China

753 Statistics Press, Beijing, 2011a.
754 National Statistical Bureau of China (NSB): China Energy Statistical Yearbook, China
755 Statistics Press, Beijing, 2011b.
756 National Statistical Bureau of China (NSB): China Industry Economy Statistical
757 Yearbook, China Statistics Press, Beijing, 2011c.
758 Nonferrous Metal Industry Association of China (NMIA): Yearbook of Nonferrous
759 Metals Industry of China, China Statistics Press, Beijing, 2011.

760 Pacyna, E. G., Pacyna, J. M., Sundseth, K., Munthe, J., Kindbom, K., Wilson, S.,
761 Steenhuisen, F., Maxson, P.: Global emission of mercury to the atmosphere from
762 anthropogenic sources in 2005 and projections to 2020, Atmos. Environ., 44,
763 2487-2499, 2010.

764 Pacyna, J. M.: Estimation of the atmospheric emissions of trace elements from
765 anthropogenic sources in Europe, Atmos. Environ., 18, 41-50, 1984.

766 Pacyna, J. M., and Pacyna, E. G.: An assessment of global and regional emissions of
767 trace metals to the atmosphere from anthropogenic sources worldwide, Environ. Rev.,
768 9, 269−298, 2001.

769 Pirrone, N., Cinnirella, S., Feng, X., Finkelman, R. B., Friedli, H. R., Leaner, J.,
770 Mason, R., Mukherjee, A. B., Stracher, G. B., Streets, D. G., Telmer, K.: Global
771 mercury emissions to the atmosphere from anthropogenic and natural sources, Atmos.
772 Chem. Phys., 10, 5951-5964, 2010.

773 Pirrone, N., Mason, R. P. (Eds): Mercury fate and transport in the global atmosphere,
774 Springer US., 2009.

775 Steenhuisen, F., Wilson, S. J.: Identifying and characterizing major emission point
776 sources as a basis for geospatial distribution of mercury emissions inventories, Atmos.
777 Environ., 112, 167-177, 2015.

778 Streets, D. G., Devane, M. K., Lu, Z., Bond, T. C., Sunderland, E.M., and Jacob, D.J.:
779 All-time releases of mercury to the atmosphere from human activities, Environ. Sci.
780 Technol., 45, 10485−10491, 2011.

781 Tang, S. L., Feng, X. B., Shang, L. H., Yan, H. Y., Hou, Y. M.: Mercury speciation and
782 emissions in the flue gas of a small-scale coal-fired boiler in Guiyang, Research of
783 Environmental Sciences, 17, 74-76, 2004 (in Chinese).

784 Tian, H. Z., Liu, K. Y., Zhou, J. R., Lu, L., Hao, J. M., Q, P. P., G, J. J., Zhu, C. Y.,
785 Wang, K., Hua, S. B.: Atmospheric Emission Inventory of Hazardous Trace Elements
786 from Chinas Coal-Fired Power Plants Temporal Trends and Spatial Variation
787 Characteristics, Environ. Sci. Technol., 48, 3575-3582, 2014.
788 Tian, H. Z., Wang, Y., Xue, Z. G., Cheng, K., Qu, Y. P., Chai, F. H., Hao, J. M.: Trend
789 and characteristics of atmospheric emissions of Hg, As, and Se from coal combustion
790 in China, 1980–2007, Atmos. Chem. Phys., 10, 11905-11919, 2010.

791 Tian, H. Z., Zhu, C. Y., Gao, J. J., Cheng, K., Hao, J. M., Wang, K., Hua, S. B., Wang,
792 Y., Zhou, J. R.: Quantitative assessment of atmospheric emissions of toxic heavy
793 metals from anthropogenic sources in China: historical trend, spatial distribution,
794 uncertainties, and control policies, Atmos. Chem. Phys., 15, 10127-10147, 2015.

795 Timmermans, R. M. A., Denier van der Gon, H. A. C., Kuenen, J. J. P., Segers, A. J.,
796 Honoré, C., Perrussel, O., Builtjes, P. J. H., Schaap, M.: Quantification of the urban
797 air pollution increment and its dependency on the use of down-scaled and bottom-up
798 city emission inventories, Urban Climate, 6, 44-62, 2013.
799 United Nations Environment Programme (UNEP): Toolkit for Identification and
800 Quantification of Mercury Releases, UNEP Chemicals Branch, 2005.
801 United Nations Environment Programme (UNEP): Toolkit for Identification and
802 Quantification of Mercury Releases, Revised Inventory Level 2 Report including
803 Description of Mercury Source Characteristics, Version 1.1., January 2011, 2011a,
804 available online at:
805 www.unep.org/hazardoussubstances/Portals/9/Mercury/Documents/Publications/Tool
806 kit/Hg%20Toolkit-Reference-Report-rev-Jan11.pdf.
807 United Nations Environment Programme (UNEP): Reducing Mercury Emissions from
808 Coal Combustion in the Energy Sector of China, Prepared for the Ministry of
809 Environment Protection of China and UNEP Chemicals, Tsinghua University, Beijing,
810 China, February 2011, 2011b, available online at:
811 www.unep.org/hazardoussubstances/Portals/9/Mercury/Documents/coal/FINAL%20C
812 hinese_Coal%20Report%20-%2011%20March%202011.pdf.
813 US Environmental Protection Agency (EPA): US National Emission Inventory 2008
814 version 2 (April 2012), 2012, available online at:
815 www.epa.gov/ttn/chief/net/2008inventory.htm.

US Geological Survey (USGS): Mercury content in coal mines in China (unpublished data), 2004.

Wang, Q. C., Shen, W. G., Ma, Z. W.: Estimation of Mercury Emission from Coal Combustion in China, Environ. Sci. Technol., 34, 2711-2713, 2000.

Wang, L., Wang, S. X., Zhang, L., Wang, Y. X., Zhang, Y. X., Nielsen, C., McElroy, M. B., Hao, J. M.: Source apportionment of atmospheric mercury pollution in China using the GEOS-Chem model, Environ. Pollut., 190(7), 166-175, 2014.

Wang, S. X., Zhang, L., Li, G. H., Wu, Y., Hao, J. M., Pirrone, N., Sprovieri, F., Ancora, M. P.: Mercury emission and speciation of coal-fired power plants in China, Atmos. Chem. Phys., 10, 1183-1192, 2010.

Wang, Y. J., Duan, Y. F., Yang, L. G., Jiang, Y. M., Wu, C. J., Wang, Q., Yang, X. H.: Analysis of the factors exercising an influence on the morphological transformation of mercury in the flue gas of a 600MW coal-fired power plant, Journal of Engineering for Thermal Energy and Power, 04, 399-403, 2008 (in Chinese).

Wang, F. Y., Wang S. X., Zhang, L., Yang, H., Gao, W., Wu, Q. R., Hao, J. M.: Mercury mass flow in iron and steel production process and its implications for mercury emission control, Journal of Environmental Sciences, 2016 (in press), available online at: http://dx.doi.org/10.1016/j.jes.2015.07.019.

Wu, Q. R., Wang, S. X., Zhang, L., Song, J. X., Yang, H., Meng, Y.: Update of mercury emissions from China's primary zinc, lead and copper smelters, 2000–2010, Atmos. Chem. Phys., 12, 11153-11163, 2012.

Xie, X., Yin, W.: Nanjing Thermal Power Plant Boiler Flue Gas Mercury Emissions in the Survey, Environmental Monitoring and Forewarning, 6, 47-49, 2014.

Yang, H.: Study on atmospheric mercury emission and control strategies from cement production in China, M.S. thesis, Tsinghua University, Beijing, China, 2014 (in Chinese).

Yao, W., Qu, X. H., Li, H. X., Fu, Y. F.: Production, collection and treatment of garbage in rural areas in China, Journal of Environment and Health, 26, 10-12, 2009 (in Chinese).

Zhang, L.: Emission Characteristics and Synergistic Control Strategies of

847 Atmospheric Mercury from Coal Combustion in China, Ph. D thesis, Tsinghua
848 University, Beijing, China, 2012 (in Chinese).

849 Zhang, L.: Research on mercury emission measurement and estimate from
850 combustion resources (Master Thesis), Zhejiang University, Hangzhou, China, 2007
851 (in Chinese).

852 Zhang, L., Wang, S. X., Meng, Y., Hao, J. M.: Influence of mercury and chlorine
853 content of coal on mercury emissions from coal-fired power plants in China, Environ.
854 Sci. Technol., 46, 6385-6392, 2012.

855 Zhang, L., Wang, S. X., Wang, L., Wu, Y., Duan, L., Wu, Q. R., Wang, F. Y., Yang, M.,
856 Yang, H., Hao, J. M., Liu, X.: Updated Emission Inventories for Speciated
857 Atmospheric Mercury from Anthropogenic Sources in China, Environ. Sci. Technol,
858 49, 3185−3194, 2015.

859 Zhao, Y., Wang, S. X., Duan, L., Lei, Y., Cao, P. F., Hao, J. M.: Primary air pollutant
860 emissions of coal-fired power plants in China: current status and future prediction,
861 Atmos. Environ., 42, 8442-8452, 2008.

862 Zhao, Y., Nielsen, C. P., Lei, Y., McElroy, M. B., Hao, J. M.: Quantifying the
863 uncertainties of a bottom-up emission inventory of anthropogenic atmospheric
864 pollutants in China, Atmos. Chem. Phys., 11, 2295-2308, 2011.

865 Zhao, Y., Nielsen, C. P., McElroy, M. B., Zhang, L., Zhang, J.: CO emissions in
866 China: uncertainties and implications of improved energy efficiency and emission
867 control, Atmos. Environ., 49, 103-113, 2012.

868 Zhao, Y., Zhong, H., Zhang, J., Nielsen, C. P.: Evaluating the effects of China's
869 pollution controls on inter-annual trends and uncertainties of atmospheric mercury
870 emissions, Atmos. Chem. Phys., 15, 4317-4337, 2015a.

871 Zhao, Y., Qiu, L. P., Xu, R. Y., Xie, F. J., Zhang, Q., Yu, Y. Y., Nielsen, C. P., Qin,
872 H. X., Wang, H. K., Wu, X. C., Li, W. Q., Zhang, J.: Advantages of a city-scale
873 emission inventory for urban air quality research and policy: the case of Nanjing, a
874 typical industrial city in the Yangtze River Delta, China, Atmos. Chem. Phys., 15,
875 18691-18746, 2015b.

876 Zhou, Y., Zhao, Y., Mao, P., Zhang, Q., Zhang, J., Qiu, L., Yang, Y.: Development of
877 a high-resolution emission inventory and its evaluation through air quality modeling

878 for Jiangsu Province, China, Atmos. Chem. Phys. Discuss., doi:10.5194/acp-2016-567,
879 2016.
880 Zhu, J., Wang, T. J., Bieser, J., Matthias, V.: Source attribution and process analysis
881 for atmospheric mercury in East China simulated by CMAQ-Hg, Atmos. Chem. Phys.,
882 15, 8767-8779, 2015.
883 Zhu, J., Wang, T. J., Talbot, R., Mao, H.: Characteristics of atmospheric total gaseous
884 mercury (tgm) observed in urban Nanjing, China, Atmos. Chem. Phys., 12,
885 25037-25080, 2012.

TABLES

Table 1 Emission estimates for Jiangsu in 2010 and species from multi-scale inventories by sector. Recall from Section 2 the abbreviations for emission sources: CPP: coal-fired power plants; RCC: residential coal combustion; O&G: oil and gas combustion; OIB: other industrial coal combustion; CEM: cement production; ISP: iron & steel plants; NMS: nonferrous metal smelting; AP: aluminum production; LGM: large-scale gold mining; MM: mercury mining; HC: human cremation; MSWI: municipal solid waste incineration; RSWI: rural solid waste incineration; BFLP: battery/fluorescent lamp production; BIO: biofuel use/biomass open burning; and PVC: PVC production.

		CPP[1]	RCC[3]	O&G[3]	OIB[1]	CEM[1]	ISP[1]	NMS[2]	AP[2]	LGM	MM	HC[3]	MSWI[2]	RSWI[3]	BFLP[2]	BIO[3]	PVC[2]	Total
Hg^T	Bottom-up	11549	195	930	8652	9264	5654	91	29	0	0	326	1009	365	158	461	423	39106
	NJU	11208	165	930	6901	1137	2243	2158	/	23	51	/	1009	457	1225	500	2603	30610
	THU	10768	345	752	10680	8238	2539	0	29	0	0	326	2294		244	219	/	36434
	BNU	12883	267	898	10172	3288	2669	2022	6		/		308			303	/	32816
	AMAP/UNEP		9292 [a]					17759 [b]						4976 [c]			/	32027
	EDGARv4.tox2	10233[d]	1181[e]	/	3310[f]	6364	447	413		/			1017		/	43	/	23008
Hg^0	Bottom-up	8811	91	465	4689	2461	1908	45	23	0	0	313	131	47	158	350	423	19915
	NJU	8133	42	465	2042	685	1208	1189	/	16	41	/	190	393	980	380	2082	17846
	THU	7689	247	376	6995	2793	863	0	23	0	0	313	2202		244	162	/	21907
	AMAP/UNEP		4646 [a]					14207 [b]						4668 [c]			/	23521
Hg^{2+}	Bottom-up	2653	73	372	3394	6752	3746	45	4	0	0	0	868	314	0	23	0	18244
	NJU	2900	45	372	4003	431	835	963	/	7	8	/	868	59	184	25	390	11090
	THU	3058	92	301	3471	5338	1676	0	4	0	0	0	0		0	11	/	13951
	AMAP/UNEP		3717 [a]					2707 [b]						238 [c]			/	6662
Hg^p	Bottom-up	85	32	93	569	51	0	0	1	0	0	13	10	4	0	88	0	946
	NJU	175	79	93	855	20	200	6	/	0	3	/	10	5	61	95	130	1732
	THU	22	6	75	214	107	0	0	1	0	0	13	92		0	46	/	576
	AMAP/UNEP		929 [a]					845 [b]						70 [c]			/	1844

[1, 2, 3] Sectors in category 1, 2 and 3 as classified in Section 2. [a] Stationary combustion sources: power plants, distributed heating, and other energy use (industrial sources excluded). [b] Industrial sources including stationary combustion for industry, CEM, ISP, NMS, AP, LGM and MM. [c] Intentional use and product waste associated sources: artisanal and small-scale gold mining, solid waste incineration and other product waste disposal, chlor-alkali industry, and human cremations. [d, e, f] Both coal and other fossil fuel combustion included.

Table 2 Hg speciation profiles by sector and the mass fractions to total emissions in multi-scale inventories (%).

Sector	Provincial inventory			NJU			THU			AMAP/UNEP		
	Hg^0	Hg^{2+}	Hg^p	Hg^0	Hg^{2+}	Hg^p	Hg^0	Hg^{2+}	Hg^p	Hg^0	Hg^{2+}	Hg^p
CPP	76	23	1	73	26	2	71	28	0	50	40	10
RCC	46	37	16	25	27	48	71	27	2	50	40	10
O&G	50	40	10	50	40	10	50	40	10	50	40	10
OIB	54	39	7	30	57	13	66	33	2	50	40	10
CEM	27	73	1	60	38	2	34	65	1	80	15	5
ISP	34	66	0	54	37	9	34	66	0	80	15	5
NMS	50	50	0	55	45	0		/		80	15	5
AP	80	15	5		/		80	15	5	80	15	5
LGM				70	30	0				80	15	5
MM		/		80	15	5		/		80	20	0
ASGM					/					100	0	0
HC	96	0	4				96	0	4	80	15	5
MSWI	13	86	1	13	86	1	96	0	4	20	60	20
BFLP	100	0	0	80	15	5	100	0	0	80	15	5
BIO	76	5	19	76	5	19	74	5	21		/	
PVC	100	0	0	80	15	5		/				
Total	51	47	2	57	37	6	60	38	2	73	21	6

Table 3 Hg speciation profiles used in provincial and national inventories for typical APCDs (%).

Sources		Hg speciation								
		Provincial inventory			NJU			THU		
		Hg^0	Hg^{2+}	Hg^p	Hg^0	Hg^{2+}	Hg^p	Hg^0	Hg^{2+}	Hg^p
Coal combustion	ESP	57	41	1	65	35	0	58	41	1
	FF	31	61	7	16	73	11	50	49	1
	WET	65	33	2	30	57	13	65	33	2
	CYC	30	57	14	30	57	13		/	
	ESP+FGD	83	16	0	83	16	0	84	16	1
	SCR+ESP+FGD	71	29	0	72	28	0	74	26	0
	FF+FGD	78	21	1		/		78	21	1
	No	48	34	18	24	20	56	56	34	10
CEM	DPT+DR/FF*	24	75	1	16	73	11	24	76	1
	SKT/ESP*	83	16	1	65	35	0	80	15	5
	RKT/WET*	47	51	1	30	57	14	80	15	5

*: DPT+DR, SKT and RKT for provincial and THU inventory (Zhang et al., 2015); FF, ESP and WET for NJU inventory (Zhao et al., 2015).

Table 4. Uncertainties of Hg emissions in Jiangsu in provincial and national (NJU) inventories by source, expressed as the 95% confidence intervals of central estimates.

	Sources	Hg^T	Hg^0	Hg^{2+}	Hg^p
Provincial	CPP	(-59%, +147%)	(-64%, +131%)	(-56%, +244%)	(-43%, +418%)
	CEM	(-15%, +58%)	(-36%, +87%)	(-18%, +63%)	(-57%, +218%)
	ISP	(-38%, +53%)	(-33%, +156%)	(-62%, +44%)	/
	OIB	(-52%, +138%)	(-55%, +133%)	(-55%, +146%)	(-67%, +329%)
	Rest sources	(-25%, +133%)	(-20%, +151%)	(-67%, +168%)	(-43%, +367%)
	Total	(-26%, +81%)	(-34%, +99%)	(-23%, +68%)	(-34%, +270%)
NJU	CPP	(-80%, +198%)	(-80%, +198%)	(-80%, +201%)	(-75%, +477%)
	CEM	(-62%, +97%)	(-75%, +140%)	(-63%, +82%)	(-73%, +266%)
	ISP	(-81%, +167%)	(-82%, +157%)	(-82%, +170%)	(-81%, +250%)
	OIB	(-83%, +153%)	(-97%, +218%)	(-97%, +228%)	(-87%, +170%)

FIGURES

Fig. 1. The ratios of estimated Hg emissions for Jiangsu 2010 in global/national inventories to that in provincial inventory for selected sources and anthropogenic total.

Fig. 2. Sensitivity analysis of selected parameters in Hg emission estimation for Category 1 sources. (a) Relative changes in parameters, calculated using Eq. (6); (b) Changes in emissions when parameters in the provincial inventory were replaced with those in other inventories, calculated using Eq. (7). HgC_{raw}: Hg content in raw coal; AL: activity levels as raw coal consumption by CPP and OIB, limestone used by CEM, and crude steel produced in ISP; TA: total abatement rate of APCDs; RR: Hg release rate for combustion; IEF: input emission factors (before control of APCDs); UEF: uniform emission factor (without consideration of different APCD types); EF_{iron} and EF_{steel}: emission factors of pig-iron and steel production respectively.

Fig. 3. Spatial distribution of Hg emissions for Jiangsu 2010 at a resolution of $0.05^o \times 0.05^o$ for (a) Hg^T, (b) Hg^0, (c) Hg^{2+}, and (d) Hg^p.

Fig. 4. Differences in gridded Hg^T emissions in Jiangsu 2010 between provincial and other inventories: emissions in provincial inventory minus those in NJU (a), THU (b), AMAP/UNEP (c) and EDGARv4.tox2 (d). The locations of point sources with relatively large Hg emissions estimated in provincial inventory are indicated in the panels as well.

Fig. 1

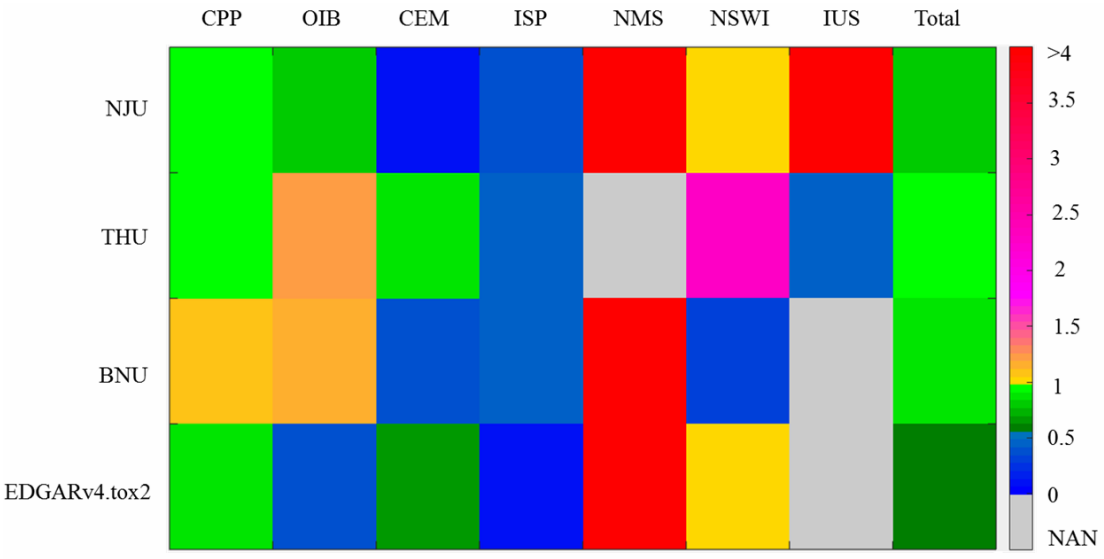
CPP
OIB
CEM
ISP
NMS
NSWI
IUS
Total
NJU
THU
BNU
EDGARv4.tox2
>4
3.5
3
2.5
2
1.5
1
0.5
0
NAN

Fig. 2.

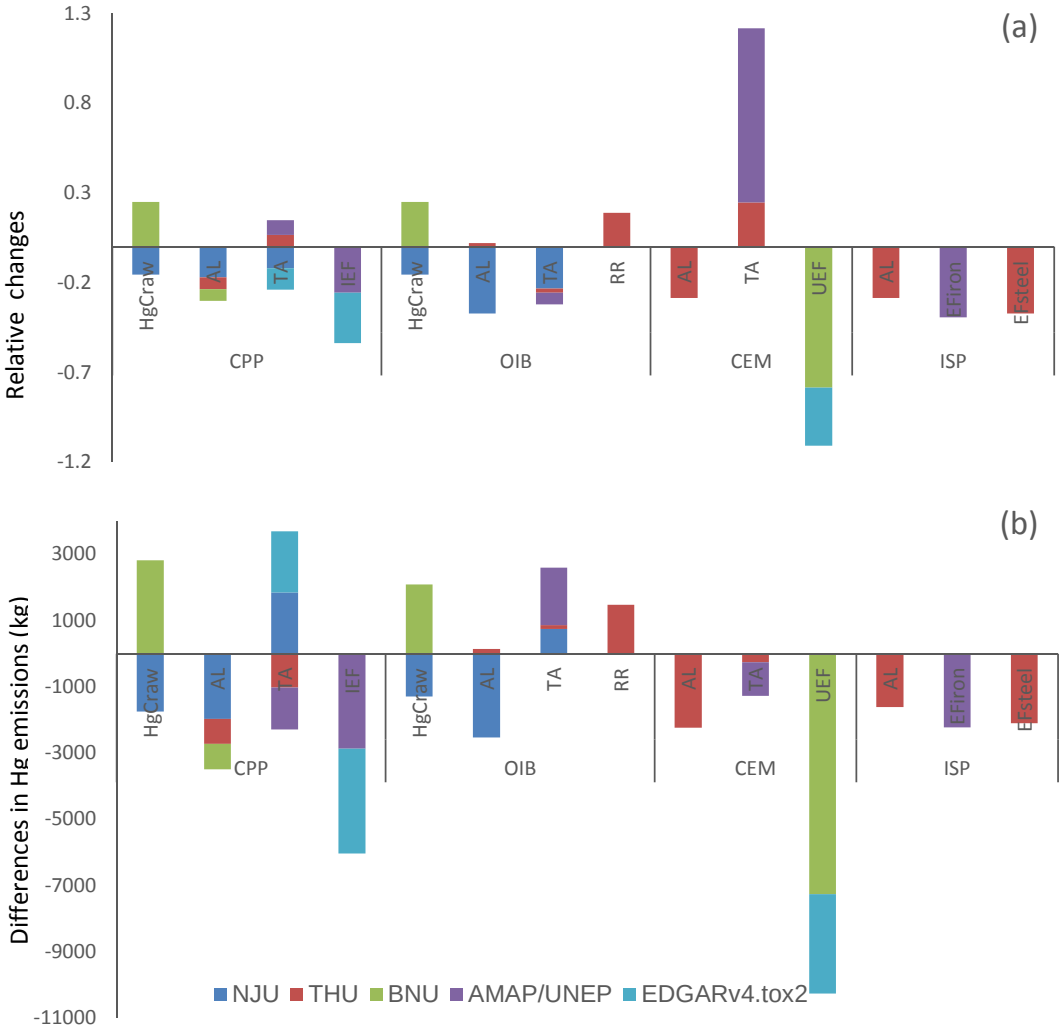
(a)
Relative changes
1.3
0.8
0.3
-0.2
-0.7
-1.2
HgCraw
AL
TA
IEF
HgCraw
AL
TA
RR
AL
TA
UEF
AL
EFiron
EFsteel
CPP
OIB
CEM
ISP
(b)
Differences in Hg emissions (kg)
3000
1000
-1000
-3000
-5000
-7000
-9000
-11000
HgCraw
AL
TA
IEF
HgCraw
AL
TA
RR
AL
TA
UEF
AL
EFiron
EFsteel
CPP
OIB
CEM
ISP
NJU
THU
BNU
AMAP/UNEP
EDGARv4.tox2

Fig. 3.

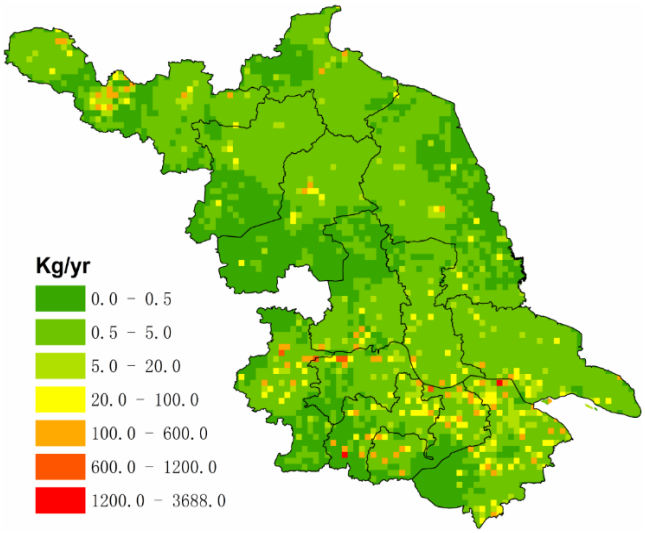

(a) Hg^T

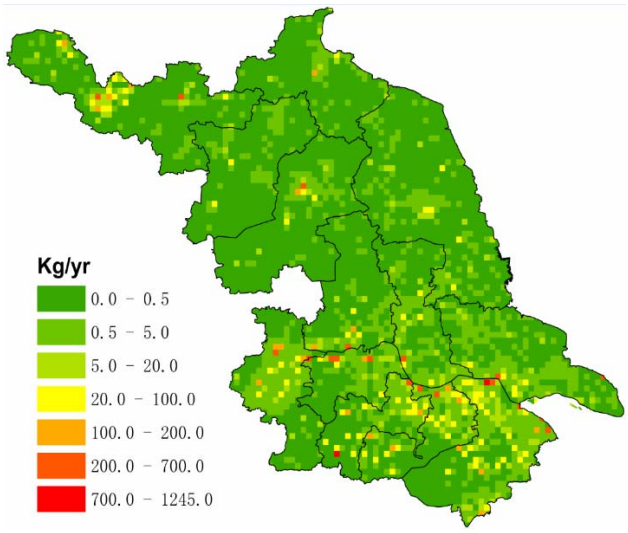

(b) Hg^0

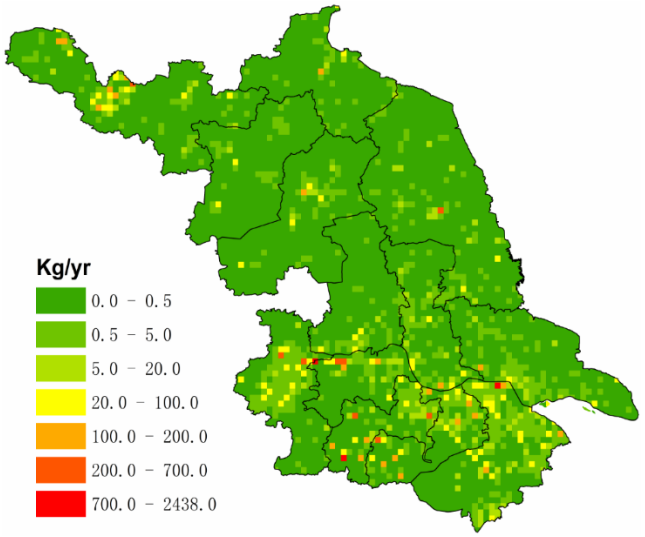

(c) Hg^{2+}

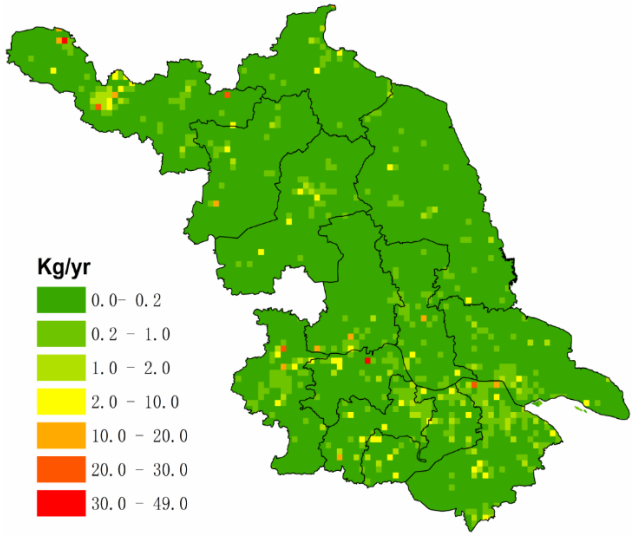

(d) Hg^p

Fig. 4.

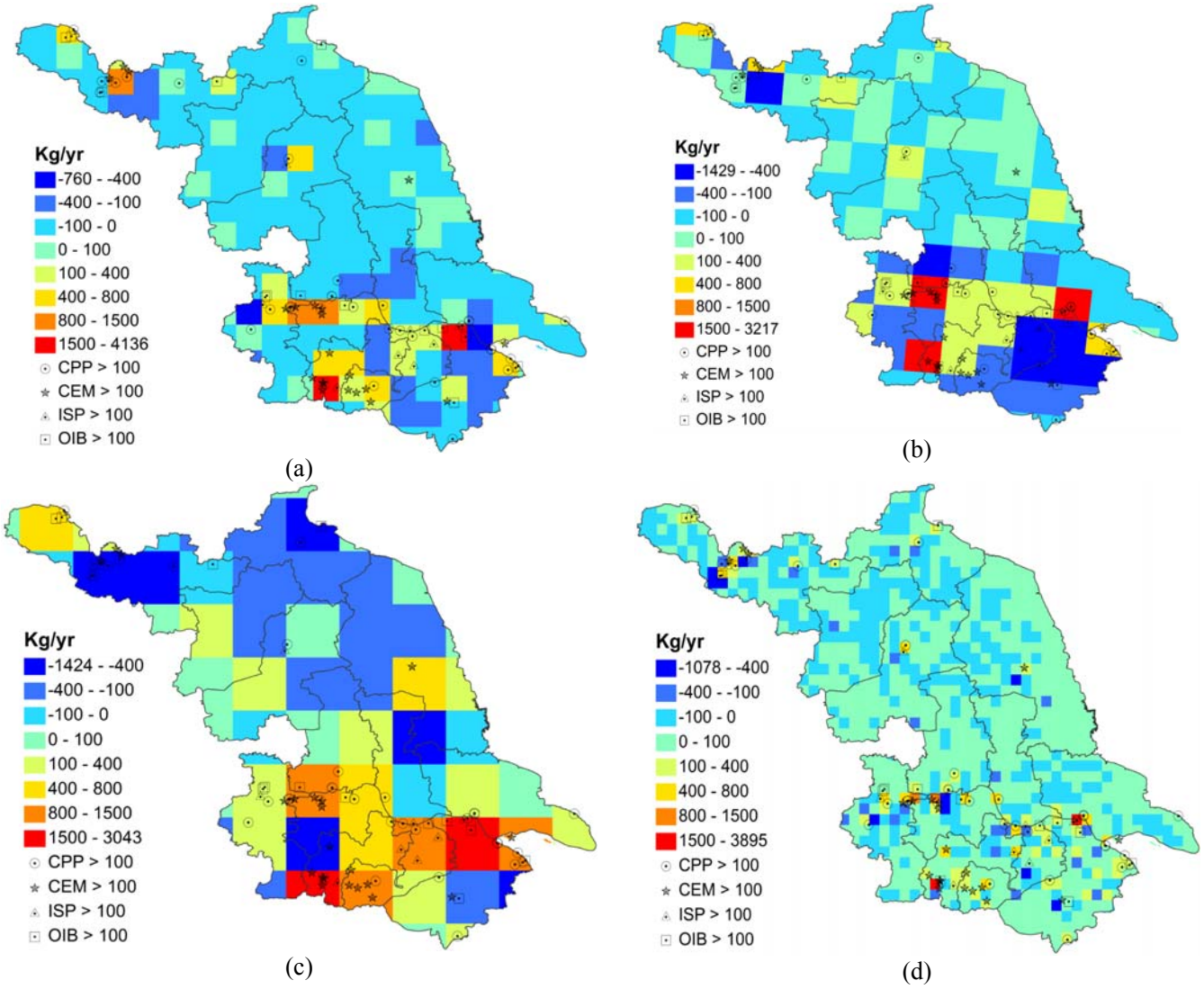
Kg/yr
-760 - -400
-400 - -100
-100 - 0
0 - 100
100 - 400
400 - 800
800 - 1500
1500 - 4136
CPP > 100
CEM > 100
ISP > 100
OIB > 100
(a)
Kg/yr
-1429 - -400
-400 - -100
-100 - 0
0 - 100
100 - 400
400 - 800
800 - 1500
1500 - 3217
CPP > 100
CEM > 100
ISP > 100
OIB > 100
(b)
Kg/yr
-1424 - -400
-400 - -100
-100 - 0
0 - 100
100 - 400
400 - 800
800 - 1500
1500 - 3043
CPP > 100
CEM > 100
ISP > 100
OIB > 100
(c)
Kg/yr
-1078 - -400
-400 - -100
-100 - 0
0 - 100
100 - 400
400 - 800
800 - 1500
1500 - 3895
CPP > 100
CEM > 100
ISP > 100
OIB > 100
(d)